



# Volcanic plumbing filters on ocean-island basalt geochemistry

Teresa Ubide<sup>1\*</sup>, Patricia Larrea<sup>2</sup>, Laura Becerril<sup>3</sup> and Carlos Galé<sup>4</sup>

<sup>1</sup>School of Earth and Environmental Sciences, The University of Queensland, Brisbane, 4072 QLD, Australia

<sup>2</sup>Department of Geology and Andean Geothermal Center of Excellence (CEGA), Universidad de Chile, 8370450 Santiago, Chile

<sup>3</sup>Instituto de Ciencias de la Ingeniería, Universidad de O'Higgins, 2841935 Rancagua, Chile

<sup>4</sup>Área de Geología, IDEYA, 50003 Zaragoza, Spain

## ABSTRACT

Ocean-island basalts (OIBs) are considered to be messengers from the deep mantle, yet the filtering effect of the plumbing systems that bring OIB melts to the surface remains poorly assessed. We investigated volcanic products from El Hierro island (Canary Islands) from textural and chemical perspectives. The majority of geochemical data cluster at relatively fractionated basaltic compositions of 5 wt% MgO. Compositions  $\geq$ 10 wt% MgO are porphyritic whole rocks that accumulate mafic minerals. Near-primary melts do not erupt. Instead, we show that carrier melts (crystal-free whole rocks, glasses, and melt inclusions) are consistently buffered to low-MgO compositions during passage through the plumbing system. We tested our model of melt fractionation and crystal accumulation on a global compilation of OIBs. Similar to El Hierro, the majority of data cluster at evolved compositions of 5 wt% MgO (alkaline) to 7 wt% MgO (tholeiitic). Modeling the fractionation of OIB parental melts, we show that with 50% crystallization, OIB melts reach 5 wt% MgO with reduced density, increased volatile content, and overall low viscosity, becoming positively buoyant relative to wall rocks and highly eruptible when reaching volatile saturation at depths around the crust–mantle boundary. Under these conditions, 5 wt% MgO OIB “sweet spot” melts are propelled to the surface and erupt carrying an assortment of recycled crystals. This mechanism is consistent with the petrography and chemistry of erupted products and suggests OIB volcanoes are dominated by low-MgO basaltic melts.

## INTRODUCTION

Volcanoes are surface expressions of complex pathways of magma transport and storage. Erupted crystals hold protracted records of pre-eruptive processes, which also modify carrier melts. However, compared to crystal records (Ganne et al., 2018), less attention has been placed on the filtering effect of the plumbing system on erupted melts (Hartley and Macلنан, 2018). This is particularly relevant for ocean-island basalts (OIBs), with chemistries long recognized to reflect melt generation in the garnet stability field at great mantle depths (Budahn and Schmidt, 1985; O’Neill, 2016). OIBs have therefore been used as a probe into the deep mantle; however, fractionation and mixing en route to the surface also contribute to OIB geochemical variability (Neumann et al., 1999; Gleeson and Gibson, 2019). In fact,

picrotic (high-MgO) parental melts are rarely sampled in glass form (Clague et al., 1991). Primitive melts in equilibrium with mantle olivine are reconstituted by correcting whole-rock compositions for olivine fractionation (e.g., Dasgupta et al., 2010). However, accumulation of mafic minerals such as olivine is common and skews bulk-rock chemistries toward MgO-rich end members (Wright and Fiske, 1971; Norman and Garcia, 1999; Larrea et al., 2013; Magee et al., 2021). Assessing the extent to which whole rocks represent liquid compositions is of critical importance in untangling the structure and composition of OIB systems, and volcanic settings in general.

To examine the geochemical makeup of OIB magmas, we combined detailed textural observations and geochemical data throughout the stratigraphy of El Hierro island (Canary Islands), and other OIB provinces worldwide. El Hierro offers a complex OIB plumbing sys-

tem (Klügel et al., 2015) and outstanding exposures of feeder dikes and associated lava flows that illustrate the effect of crystal accumulation on bulk-rock compositions (Fig. 1). Porphyritic rocks rich in olivine and clinopyroxene have almost twice the MgO content relative to aphyric samples within the same lava-dike system. In contrast, dike-flow pairs with similar textures are geochemically indistinguishable. The potential overprint of primary signatures by accumulation of recycled crystals calls for careful petrographic assessment of OIB elemental patterns, which has been lacking to date. In this study, we explored the petrographic controls on the interpretation of OIB chemistries and their implications for the composition and architecture of the oceanic crust in OIB settings.

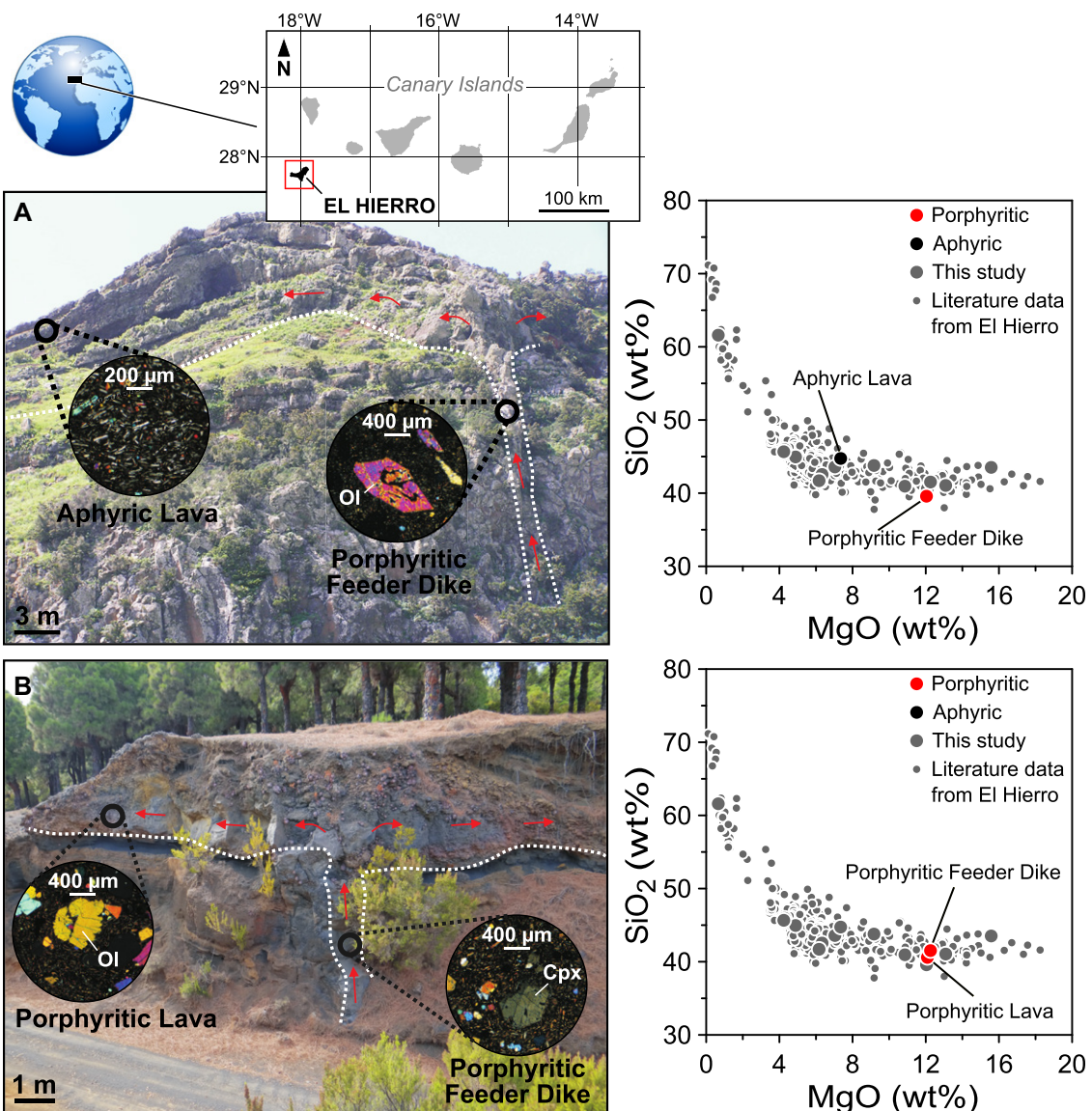
## MELT FRACTIONATION AND CRYSTAL ACCUMULATION

We analyzed 16 new bulk-rock vesiculated samples across the onshore stratigraphy of El Hierro for major and selected trace elements via X-ray fluorescence (XRF) (sample locations and methods are provided in the Supplemental Material<sup>1</sup>). We combined these data with 415 published geochemical analyses from El Hierro, including the recent 2011–2012 CE submarine eruption (Fig. S1 in the Supplemental Material). Our data set (Table S1) includes a careful evaluation of sample petrography, based on inspection of available samples and published literature. We divided samples into “porphyritic” and “aphyric” based on the presence and absence of phenocrysts, respectively, which included olivine, clinopyroxene, and minor Fe-Ti oxides (Table S2; see also Carracedo et al., 2001). Instances of ambiguous texture were named “unknown.” Matrix glass was included in the aphyric group, separate from olivine- and clinopyroxene-hosted “melt inclusions” (corrected

\*E-mail: t.ubide@uq.edu.au

<sup>1</sup>Supplemental Material. Data (Tables S1–S8), methods, and Figures S1–S3. Please visit <https://doi.org/10.1130/GEOL.S.15832080> to access the supplemental material, and contact editing@geosociety.org with any questions.

CITATION: Ubide, T., et al., 2021, Volcanic plumbing filters on ocean-island basalt geochemistry: *Geology*, v. 50, p. 26–31, <https://doi.org/10.1130/G49224.1>



for post-entrapment crystallization and diffusive reequilibration, and limited to corrections of <10%; Longpré et al., 2017; Taracsák et al., 2019).

The frequency distribution of MgO in El Hierro samples defines a major peak at ~5 wt% MgO, which broadly agrees with the change in slope of geochemical trends in bivariate diagrams (Fig. 2). Traditionally, the decrease in MgO has been linked to fractional crystallization from high-MgO parental melts, with kinks in trends related to changes in the fractionating assemblage (Fig. 2A). However, our petrographic assessment indicates that compositions ≥10 wt% MgO are cumulates with high volume fractions of clinopyroxene and particularly olivine (~25%; Table S2). The carrier melts, represented by aphyric bulk rocks, glasses, and melt inclusions, are relatively evolved basanites that cluster at the dominant 5 wt% MgO peak. Melt inclusions reach up to ~8 wt% MgO only, even if they are hosted in mafic phases crystallized at

mantle depths (Taracsák et al., 2019), supporting the notion that bulk rocks with high MgO do not represent magmatic liquids.

To explain the geochemical variations in a manner consistent with rock textures, we propose a new model of combined melt fractionation and crystal accumulation (Fig. 2B). Taking an aphyric rock with ~5 wt% MgO as representative of basaltic liquids at El Hierro, we modeled accumulation vectors of 20% olivine, clinopyroxene, and plagioclase, and 5% titanomagnetite via mass balance. Variations in mineral and liquid compositions will modify accumulation models slightly, but the overall magnitude and direction of mineral vectors hold. Together, accumulation of olivine, clinopyroxene, and minor titanomagnetite induces  $MgO-CaO-Fe_2O_3$  enrichment and  $TiO_2-Al_2O_3$  depletion at constant  $SiO_2$ , as defined by the porphyritic trend (Fig. 2; Fig. S2; Table S3). This is in agreement with the crystal cargo observed in porphyritic samples, which typically lack

plagioclase phenocrysts. Least-squares modeling of porphyritic rocks via MINSQ (Herrmann and Berry, 2002) returned proportions of constituent phases that agree with the petrographic observations, with low residuals (Table S4). The trace-element variability of crystal-rich samples also agrees with accumulation of mafic minerals. Porphyritic data define increasing Ni–Cr trajectories with increasing MgO, while elements and elemental ratios insensitive to olivine and clinopyroxene, such as Sr, Zr, Y, and Zr/Nb, remain constant (Fig. S3). The correlations between crystal-rich textures and high-MgO compositions indicate entrainment of recycled crystals (antecrysts) as the main driver of chemical diversity of porphyritic samples. Crystal recycling is closely related to magma mixing, which has been widely documented by the broad compositional spectrum of mineral zonations and melt inclusions in recent El Hierro products (Stronckik et al., 2009; Longpré et al., 2014; Taracsák et al., 2019). It follows that erupted melts at El

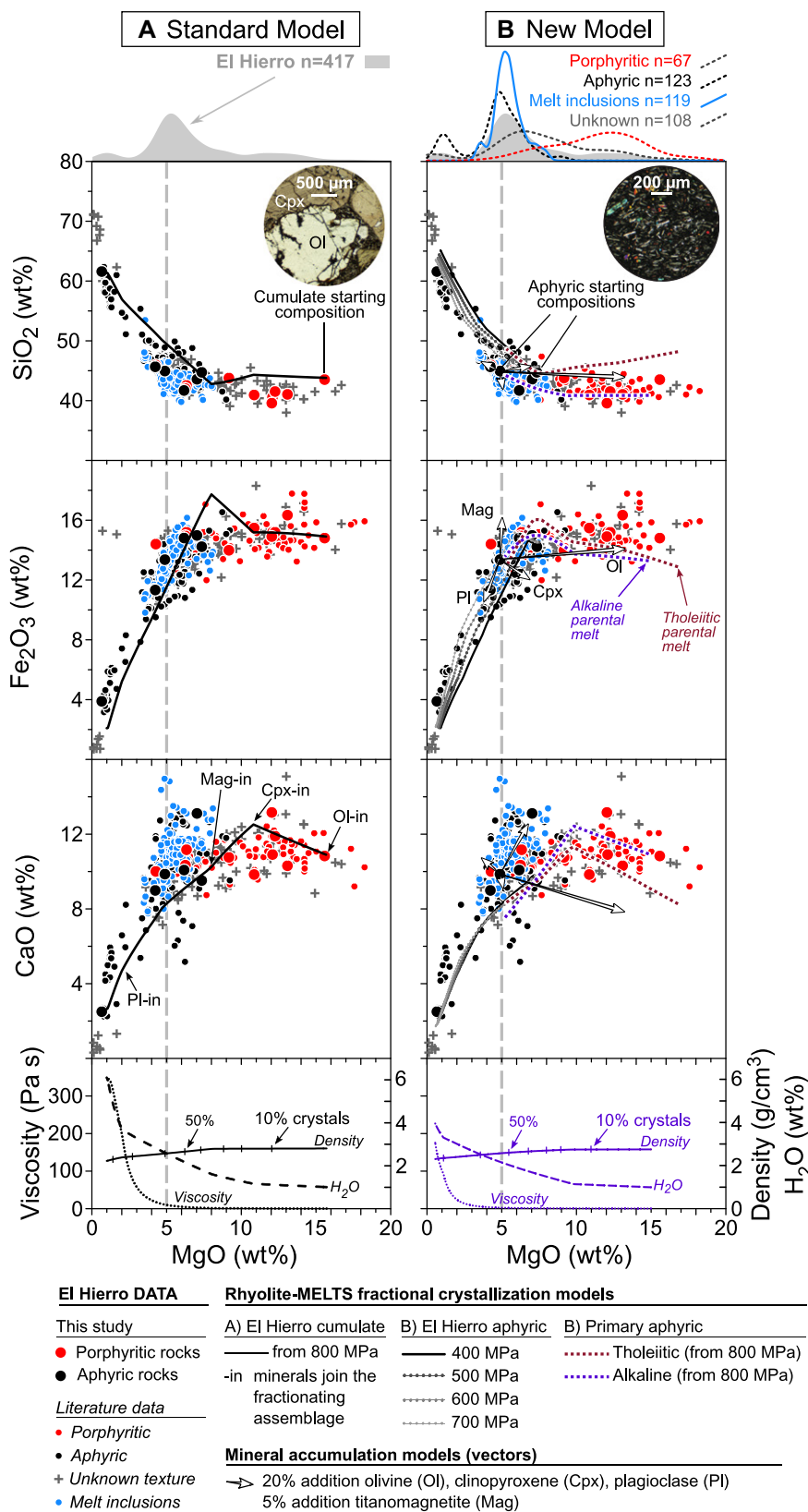


**Figure 2.** Geochemistry of El Hierro island (Canary Islands) explained via (A) standard fractional crystallization from high-MgO bulk-rock compositions, and (B) fractional crystallization and crystal accumulation using crystal-free basaltic compositions as proxies for liquids. Frequency curves of MgO concentration (kernel density plots) show major peak at 5 wt% for aphric bulk rocks (cross-polarized light photomicrograph, sample LDAEH3), glasses, and melt inclusions. Porphyritic samples peak at  $\geq 10$  wt% MgO, reflecting crystal accumulation (in plane-polarized light photomicrograph, sample TIMBAS3; Ol—olivine, Cpx—clinopyroxene). Database, textural data, and models are given in the Supplemental Material (see footnote 1).

Hierro are buffered to nonprimary compositions and incorporate a mix of mafic antecysts while traveling to the surface.

To link 5 wt% MgO compositions with parental OIB melts, we invoke cryptic fractional crystallization, which is largely unseen in the chemistry of erupted aphric rocks and glasses. We started with a primary melt calculated from the most magnesian OIB glasses yet found (14.7 wt% MgO tholeiitic glasses from Kilauea, Hawaii, reconstituted to 17 wt% MgO in equilibrium with primary olivine; Clague et al., 1991). We also used a primary melt calculated from alkaline glasses from Kilauea (pre-shield stage 6.4 wt% MgO glass, reconstituted to 15 wt% MgO in equilibrium with peridotitic olivine; Sisson et al., 2009). Polybaric fractionation from 800 MPa (27 km depth assuming a combined crust-mantle density of 3 kg/m<sup>3</sup>) via rhyolite-MELTS (Gualda et al., 2012) reduced the MgO of the melt to 5 wt% at mantle depths equivalent to  $\sim 600$  MPa after 50% crystallization (Fig. 2B; Table S5), reproducing the compositional peak at El Hierro.

Phase equilibria experiments, clinopyroxene-melt barometry, and fluid and melt inclusion data (Hansteen and Klügel, 2008; Stronck et al., 2009; Martí et al., 2013; Longpré et al., 2014, 2017; Klügel et al., 2015; Taracsák et al., 2019) indicate that El Hierro melts evolve at upper-mantle conditions. Isobaric fractional crystallization between 400 and 700 MPa from our most primitive aphric sample ( $\sim 7$  wt% MgO) produced liquid lines of descent that mirror natural phenocryst-free compositions (aphric samples and melt inclusions; Fig. 2B). We favor the model at 400 MPa ( $\sim 14$  km, near the crust-mantle boundary according to geophysical data of Ranero et al. [1995]) because the fractionated phases and compositions closely match the mineral assemblage of eruptive products (Table S5). This is in agreement with the hypocentral location of seismicity preceding the 2011–2012 eruption (dominantly at 12–15 km depth), suggesting magma accumulation and migration near the base of the crust (López et al., 2012).

## GLOBAL OIBS AS NONPRIMITIVE LIQUIDS

Remarkably, patterns of MgO distribution and major-element oxide relationships similar to El Hierro arise at other OIBs globally (Fig. 3; cf. Table S6 for data compilation, mostly from subaerial exposures). Many locations show a major peak at  $\sim 5$  and a smaller population at  $\geq 10$  wt% MgO (for example, Cape Verde [South Atlantic Ocean], and the Marquesas Islands and Samoa [South Pacific Ocean]), while in certain island groups (such as the Azores, Madeira, and St. Helena [Atlantic Ocean]), the frequency distribution is more even. This could reflect differences in melting conditions (Humphreys and

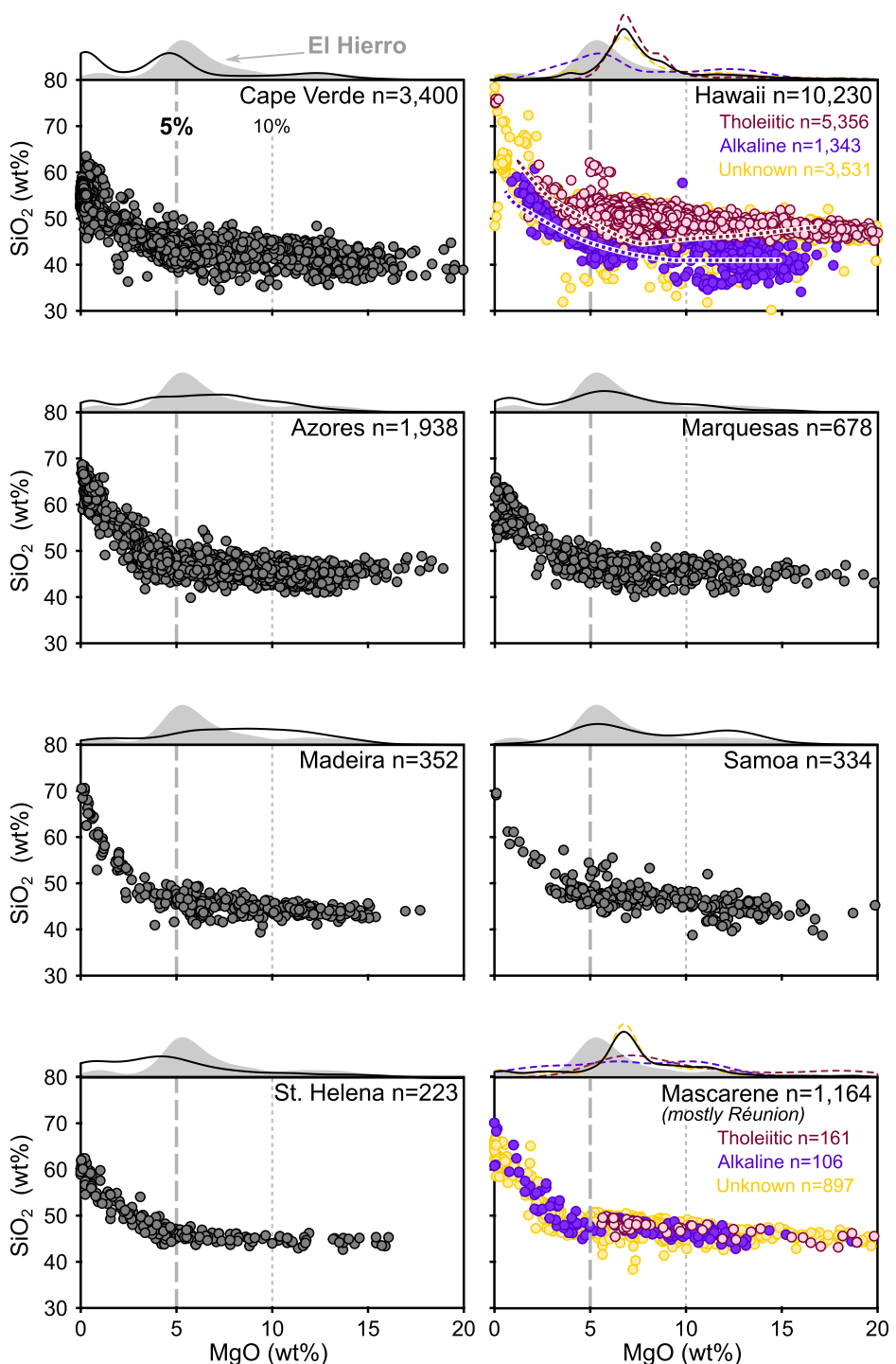


**Figure 3.** Ocean-island bulk-rock and glass compositions across the Atlantic, Pacific, and Indian Oceans (Table S6 [see footnote 1]), including probability density curves of MgO content in each system (kernel density plots). El Hierro island (Canary Islands) curves are included for context. Alkaline ocean-island basalts (OIBs) peak around 5 wt% MgO, and tholeiitic OIBs peak at 7 wt% MgO. High-MgO compositions are interpreted to reflect crystal accumulation, as seen at El Hierro. For ease of comparison, x axes are as in Figure 2; however, data >20 wt% MgO are common in tholeiite cumulates from Hawaii and Réunion (Mascarene). Hawaii modeling is the same as in Figure 2, and extended below 5 wt% MgO (800–400 MPa trends).

Niu, 2009) and mantle heterogeneity (Dasgupta et al., 2010), but also differences in the extent of crystal accumulation and fractional crystallization amongst islands. For example, historical eruptions at Lanzarote (Canary Islands) pro-

duced olivine- and ultramafic xenolith-bearing porphyritic products (Gómez-Ulla et al., 2018) that skew bulk-rock compositions to the MgO-rich end of the spectrum. The high carrying capacity of some OIB volcanoes may relate to

high magmatic CO<sub>2</sub> contents, which can exsolve at great depth (Edmonds and Woods, 2018), disaggregating and rapidly erupting dense cargoes. The “crystal effect” on high-MgO compositions is common across OIBs, with significant proportions of data at  $\geq 10$  wt% MgO (Fig. 3) and abundant literature descriptions of strongly phryic samples (Table S7).

In areas of high melt generation such as Hawaii (Pacific Ocean) and Réunion (Indian Ocean), the main compositional group is shifted to  $>5$  wt% MgO (Fig. 3). This shift is associated with an abundance of tholeiites; i.e., products of higher extents of mantle melting and more mafic magmas ( $\sim 7$  wt% MgO peak) than the alkaline magmas that dominate other OIBs ( $\sim 5$  wt% MgO peak). The MgO distribution in OIB tholeiites is similar to that of mid-oceanic ridge basalts (MORB) glass averages 7.6 wt% MgO with 50% crystallization; O’Neill and Jenner, 2012). Those authors showed that the compositional variability of ocean-floor tholeiites is buffered by the cycling of magma through chambers via recharge, mixing, crystallization, and eruption, in agreement with our findings for OIBs.

The striking global observation that many OIBs share a compositional peak at low MgO contents of  $\sim 5$  wt% suggests that liquid compositions in OIB magma chambers are fractionated to low-MgO contents and become highly eruptible (Fig. 4; Table S8). Deep-seated fractionation of alkaline primary melts reduces MgO to 5 wt% after 50% crystallization. Because of the late saturation of plagioclase in OIB melts, density decreases continuously without reaching a minimum (Fig. 2), which has been linked to maximum buoyancy in other settings (Sparks et al., 1980; Stolper and Walker, 1980; Hartley and MacLennan, 2018). At 5 wt% MgO, density is lowered while viscosity remains low, and the melt is positively buoyant to crustal depths (Putirka, 2017), leading to ascent. Critically, water contents increase, and ascent to pressures of  $\sim 300$ –400 MPa may trigger volatile saturation in CO<sub>2</sub>-bearing magmas such as those at El Hierro (Longpré et al., 2017) and other OIBs (Edmonds and Woods, 2018). Vesiculation increases the buoyancy of magma by decreasing its density and viscosity (Putirka, 2017; Hartley and MacLennan, 2018) and may propel 5 wt% MgO “sweet spot” melts to the surface. Despite the addition of crystals (up to 35% following petrographic observations), which increases the density and viscosity of the magma, viscosities remain well below the eruptibility threshold of  $10^6$  Pa·s (Takeuchi, 2011). Significantly, the predicted eruptible sweet spot at 50% crystallization based on geochemical signatures is consistent with mechanical constraints on the optimal extraction window of basaltic melts at 50%–65% crystallinity (Fig. 4; Dufek and Bachmann, 2010).

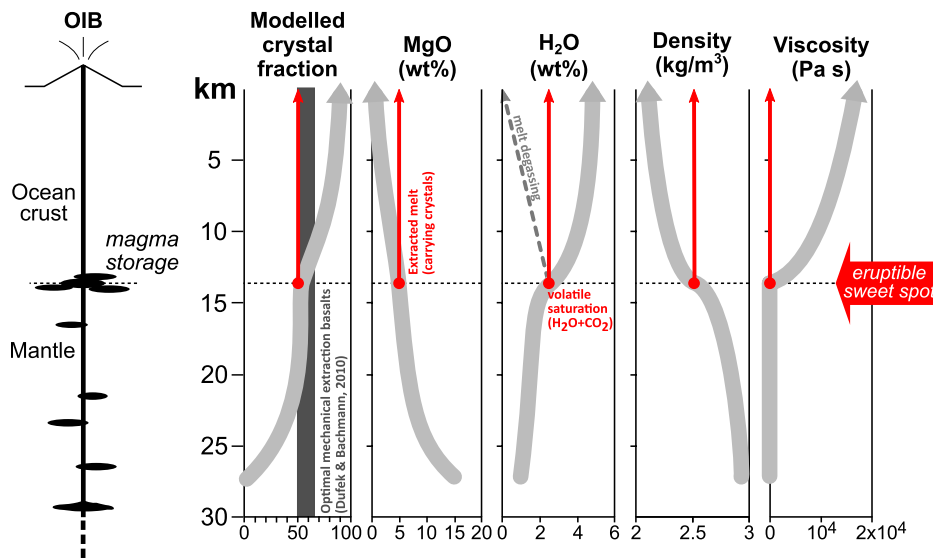


**Figure 4.** Filtering of melt compositions through the plumbing system of ocean-island volcanoes. Plots show variations in physical and chemical properties of crystal-free ocean-island basalt (OIB) melts during ascent through the upper mantle and crust, based on modeling from Hawaiian alkaline parental melts and El Hierro island (Canary Islands) compositions from this study (Table S8 [see footnote 1]). Fractional crystallization drives melt evolution down to 5 wt% MgO at upper-mantle conditions with 50% crystallization, yielding densities and viscosities that make liquids positively buoyant relative to wall rocks, and highly eruptible upon volatile saturation from Moho depths. At this compositional “sweet spot”, OIB liquids accelerate to surface, recycling mafic crystals and generating high-MgO products.

Our results reveal that liquid compositions in OIB magma chambers are relatively evolved basaltic products of picritic parental melts. This occurs during transport through vertically extended feeder systems that control the growth and evolution of OIBs (Klügel et al., 2015). Basaltic liquids with low-MgO contents (5 wt% MgO, less than half the >10 wt% MgO traditionally considered parental to OIBs) may reach volatile saturation at the base of the crust, increasing buoyancy and accelerating to the surface with a cargo of recycled crystals that obfuscate bulk-rock chemistries. Petrography is required to discriminate between petrogenetic hypotheses. Antecrust accumulation obscures whole-rock chemical data, with aphyric samples and glasses representing the best proxies for liquid compositions with which to model melting, fractionation, assimilation, and mixing. Together, our findings show the prevalent magma filtering effect of volcano plumbing systems, which may have implications for understanding crustal growth and mantle evolution in terrestrial planets.

#### ACKNOWLEDGMENTS

This work greatly benefited from supportive and insightful reviews by O. Bachmann, H. O’Neill, K. Putirka, and an anonymous reviewer. We thank J. Caulfield and H. Bostock for informal critique, and A. Jeffery and R. Gertisser for their compilation of Atlantic ocean-island basalts. We acknowledge funding from the Spanish Geological Survey (Instituto Geológico y Minero de España, L. Becerril); the University of Queensland and the Queensland Government, Australia (UQ-FREA RM2019001828 and WRAP109-2019RD1, T. Ubide); and Universidad

de Chile (Facultad de Ciencias Físicas y Matemáticas, P. Larrea). We dedicate the work to our years of friendship and collaboration, and to Bruno, Arnau, and Garoé, all born during the gestation of this manuscript.

#### REFERENCES CITED

- Budahn, J.R., and Schmidt, R.A., 1985, Petrogenetic modeling of Hawaiian tholeiitic basalts: A geochemical approach: *Geochimica et Cosmochimica Acta*, v. 49, p. 67–87, [https://doi.org/10.1016/0016-7037\(85\)90192-9](https://doi.org/10.1016/0016-7037(85)90192-9).
- Carracedo, J.C., Rodríguez Badiola, E., Guillou, H., de la Nuez, J., and Pérez Torrado, F.J., 2001, Geology and volcanism of La Palma and El Hierro, Western Canaries: *Estudios Geológicos*, v. 57, p. 175–273, <https://doi.org/10.3989/egeol.01575-6134>.
- Clague, D.A., Weber, W., and Dixon, J., 1991, Picritic glasses from Hawaii: *Nature*, v. 353, p. 553–556, <https://doi.org/10.1038/353553a0>.
- Dasgupta, R., Jackson, M.G., and Lee, C.-T.A., 2010, Major element chemistry of ocean island basalts—Conditions of mantle melting and heterogeneity of mantle source: *Earth and Planetary Science Letters*, v. 289, p. 377–392, <https://doi.org/10.1016/j.epsl.2009.11.027>.
- Dufek, J., and Bachmann, O., 2010, Quantum magmatism: Magmatic compositional gaps generated by melt-crystal dynamics: *Geology*, v. 38, p. 687–690, <https://doi.org/10.1130/G30831.1>.
- Edmonds, M., and Woods, A.W., 2018, Exsolved volatiles in magma reservoirs: *Journal of Volcanology and Geothermal Research*, v. 368, p. 13–30, <https://doi.org/10.1016/j.jvolgeores.2018.10.018>.
- Ganne, J., Bachmann, O., and Feng, X., 2018, Deep into magma plumbing systems: Interrogating the crystal cargo of volcanic deposits: *Geology*, v. 46, p. 415–418, <https://doi.org/10.1130/G39857.1>.
- Gleeson, M.L.M., and Gibson, S.A., 2019, Crustal controls on apparent mantle pyroxenite signals in ocean-island basalts: *Geology*, v. 47, p. 321–324, <https://doi.org/10.1130/G45759.1>.
- Gómez-Ulla, A., Sigmarsson, O., Huertas, M.J., Devidal, J.L., and Ancochea, E., 2018, The historical basanite–alkali basalt–tholeiite suite at Lanzarote, Canary Islands: Carbonated melts of heterogeneous mantle source?: *Chemical Geology*, v. 494, p. 56–68, <https://doi.org/10.1016/j.chemgeo.2018.07.015>.
- Gualda, G.A.R., Ghiorso, M.S., Lemons, R.V., and Carley, T.L., 2012, Rhyolite-MELTS: A modified calibration of MELTS optimized for silica-rich, fluid-bearing magmatic systems: *Journal of Petrology*, v. 53, p. 875–890, <https://doi.org/10.1093/petrology/egr080>.
- Hanstee, T.H., and Klügel, A., 2008, Fluid inclusion thermobarometry as a tracer for magmatic processes: *Reviews in Mineralogy and Geochemistry*, v. 69, p. 143–177, <https://doi.org/10.2138/rmg.2008.69.5>.
- Hartley, M., and MacLennan, J., 2018, Magmatic densities control erupted volumes in Icelandic volcanic systems: *Frontiers of Earth Science*, v. 6, p. 29, <https://doi.org/10.3389/feart.2018.00029>.
- Herrmann, W., and Berry, R.F., 2002, MINSQ: A least squares spreadsheet method for calculating mineral proportions from whole-rock major element analyses: *Geochemistry: Exploration, Environment, Analysis*, v. 2, p. 361–368, <https://doi.org/10.1144/1467-787302-010>.
- Humphreys, E.R., and Niu, Y., 2009, On the composition of ocean island basalts (OIB): The effects of lithospheric thickness variation and mantle metasomatism: *Lithos*, v. 112, p. 118–136, <https://doi.org/10.1016/j.lithos.2009.04.038>.
- Klügel, A., Longpré, M.A., García-Cañada, L., and Stix, J., 2015, Deep intrusions, lateral magma transport and related uplift at ocean island volcanoes: *Earth and Planetary Science Letters*, v. 431, p. 140–149, <https://doi.org/10.1016/j.epsl.2015.09.031>.
- Larrea, P., França, Z., Lago, M., Widom, E., Galé, C., and Ubide, T., 2013, Magmatic processes and the role of antecrysts in the genesis of Corvo Island (Azores Archipelago, Portugal): *Journal of Petrology*, v. 54, p. 769–793, <https://doi.org/10.1093/petrology/egs084>.
- Longpré, M.A., Klügel, A., Diehl, A., and Stix, J., 2014, Mixing in mantle magma reservoirs prior to and during the 2011–2012 eruption at El Hierro, Canary Islands: *Geology*, v. 42, p. 315–318, <https://doi.org/10.1130/G35165.1>.
- Longpré, M.A., Stix, J., Klügel, A., and Shimizu, N., 2017, Mantle to surface degassing of carbon- and sulphur-rich alkaline magma at El Hierro, Canary Islands: *Earth and Planetary Science Letters*, v. 460, p. 268–280, <https://doi.org/10.1016/j.epsl.2016.11.043>.
- López, C., et al., 2012, Monitoring the volcanic unrest of El Hierro (Canary Islands) before the onset of the 2011–2012 submarine eruption: *Geophysical Research Letters*, v. 39, L13303, <https://doi.org/10.1029/2012GL051846>.
- Magee, R., Ubide, T., and Caulfield, J.T., 2021, Days to weeks of syn-eruptive magma interaction: High-resolution geochemistry of the 2002–03 branched eruption at Mount Etna: *Earth and Planetary Science Letters*, v. 565, p. 116904, <https://doi.org/10.1016/j.epsl.2021.116904>.
- Martí, J., Castro, A., Rodríguez, C., Costa, F., Carrasquilla, S., Pedreira, R., and Bolós, X., 2013, Correlation of magma evolution and geophysical monitoring during the 2011–2012 El Hierro (Canary Islands) submarine eruption: *Journal of Petrology*, v. 54, p. 1349–1373, <https://doi.org/10.1093/petrology/egt014>.
- Neumann, E.-R., Wulff-Pedersen, E., Simonsen, S.L., Pearson, N.J., Martí, J., and Mitjavila, J., 1999,

- Evidence for fractional crystallization of periodically refilled magma chambers in Tenerife, Canary Islands: *Journal of Petrology*, v. 40, p. 1089–1123, <https://doi.org/10.1093/petroj/40.7.1089>.
- Norman, M.D., and Garcia, M.O., 1999, Primitive magmas and source characteristics of the Hawaiian plume: Petrology and geochemistry of shield picrites: *Geochimica et Cosmochimica Acta*, v. 168, p. 27–44, [https://doi.org/10.1016/S0012-821X\(99\)00043-6](https://doi.org/10.1016/S0012-821X(99)00043-6).
- O'Neill, H.St.C., 2016, The smoothness and shapes of chondrite-normalized rare earth element patterns in basalts: *Journal of Petrology*, v. 57, p. 1463–1508, <https://doi.org/10.1093/petrology/egw047>.
- O'Neill, H.St.C., and Jenner, F.E., 2012, The global pattern of trace-element distributions in ocean floor basalts: *Nature*, v. 491, p. 698–704, <https://doi.org/10.1038/nature11678>.
- Putirka, K.D., 2017, Down the crater: Where magmas are stored and why they erupt: *Elements*, v. 13, p. 11–16, <https://doi.org/10.2113/gselements.13.1.11>.
- Ranero, C.R., Torne, M., and Banda, E., 1995, Gravity and multichannel seismic reflection constraints on the lithospheric structure of the Canary Swell: *Marine Geophysical Researches*, v. 17, p. 519–534, <https://doi.org/10.1007/BF01204342>.
- Sisson, T.W., Kimura, J.-I., and Coombs, M.L., 2009, Basanite-nephelinite suite from early Kilauea: Carbonated melts of phlogopite–garnet peridotite at Hawaii's leading magmatic edge: *Contributions to Mineralogy and Petrology*, v. 158, p. 803–829, <https://doi.org/10.1007/s00410-009-0411-8>.
- Sparks, R.S.J., Meyer, P., and Sigurdsson, H., 1980, Density variation amongst mid-ocean ridge basalts: Implications for magma mixing and the scarcity of primitive lavas: *Earth and Planetary Science Letters*, v. 46, p. 419–430, [https://doi.org/10.1016/0012-821X\(80\)90055-2](https://doi.org/10.1016/0012-821X(80)90055-2).
- Stolper, E., and Walker, D., 1980, Melt density and the average composition of basalt: *Contributions to Mineralogy and Petrology*, v. 74, p. 7–12, <https://doi.org/10.1007/BF00375484>.
- Stroncik, N.A., Klügel, A., and Hansteen, T.H., 2009, The magmatic plumbing system beneath El Hierro (Canary Islands): Constraints from phenocrysts and naturally quenched basaltic glasses in submarine rocks: *Contributions to Mineralogy and Petrology*, v. 157, p. 593–607, <https://doi.org/10.1007/s00410-008-0354-5>.
- Takeuchi, S., 2011, Preeruptive magma viscosity: An important measure of magma eruptibility: *Journal of Geophysical Research: Solid Earth*, v. 116, B10201, <https://doi.org/10.1029/2011JB008243>.
- Taracsák, Z., Hartley, M., Burgess, R., Edmonds, M., Iddon, F., and Longpré, M.A., 2019, High fluxes of deep volatiles from ocean island volcanoes: Insights from El Hierro, Canary Islands: *Geochimica et Cosmochimica Acta*, v. 258, p. 19–36, <https://doi.org/10.1016/j.gca.2019.05.020>.
- Wright, T.L., and Fiske, R.S., 1971, Origin of the differentiated and hybrid lavas of Kilauea volcano, Hawaii: *Journal of Petrology*, v. 12, p. 1–65, <https://doi.org/10.1093/petrology/12.1.1>.

Printed in USA